An Engineered Cation Site in Cytochrome *c* Peroxidase Alters the Reactivity of the Redox Active Tryptophan†

Christopher A. Bonagura, Munirathinam Sundaramoorthy, Helen S. Pappa,‡ William R. Patterson,§ and Thomas L. Poulos*

Departments of Molecular Biology & Biochemistry and Physiology & Biophysics, University of California, Irvine, California 92717-3900

Received January 18, 1996; Revised Manuscript Received March 18, 1996⊗

ABSTRACT: The crystal structures of cytochrome *c* peroxidase and ascorbate peroxidase are very similar, including the active site architecture. Both peroxidases have a tryptophan residue, designated the proximal Trp, located directly adjacent to the proximal histidine heme ligand. During the catalytic cycle, the proximal Trp in cytochrome *c* peroxidase is oxidized to a cation radical. However, in ascorbate peroxidase, the porphyrin is oxidized, not the proximal Trp, despite the close similarity between the two peroxidase active site structures. A cation located ≈8 Å from the proximal Trp in ascorbate peroxidase but absent in cytochrome *c* peroxidase is thought to be one reason why ascorbate peroxidase does not form a Trp radical. Site-directed mutagenesis has been used to introduce the ascorbate peroxidase cation binding site into cytochrome *c* peroxidase. Crystal structures show that mutants now bind a cation. Electron paramagnetic resonance spectroscopy shows that the cation-containing mutants of cytochrome *c* peroxidase no longer form a stable Trp radical. The activity of the cation mutants using ferrocytochrome *c* as a substrate is <1% of wild type levels, while the activity toward a small molecule substrate, guaiacol, increases. These results demonstrate that long range electrostatic effects can control the reactivity of a redox active amino acid side chain and that oxidation/reduction of the proximal Trp is important in the oxidation of ferrocytochrome *c*.

Many metalloenzymes operate by storing oxidizing equivalents derived from O_2 or peroxides in the active site to form relatively stable organic radicals and/or high-valence metal complexes. It long has been recognized that the protein controls where oxidizing equivalents will be stored, but the question of how remains unanswered. Because the various intermediates are stable and can be investigated using a number of biophysical techniques, peroxidases are particularly well-suited to probe the relationship between protein structure and how and where oxidizing equivalents are stored.

Peroxidases catalyze the oxidation of a variety of substrates in the following multistep reaction cycle.

$$Fe^{3+}R + H_2O_2 \rightarrow \underset{\text{compound I}}{Fe^{4+}{=}OR^{\bullet}}$$

$$Fe^{4+}{=}OR^{\bullet} + S \rightarrow Fe^{4+}{=}OR + \underset{\text{compound II}}{S^{\bullet}}$$

$$Fe^{4+}{=}OR + S \rightarrow Fe^{3+}R + S^{\bullet}$$

The enzyme first is oxidized by peroxide to give compound I. One electron is removed from the heme iron to give the $Fe^{4+}{=}O$ center, and a second electron is removed from an active site group, R, in the above scheme. In most heme peroxidases, $R^{\bullet}$ is a porphyrin π cation radical (Dolphin *et al*., 1971), although in cytochrome *c* peroxidase (CCP),[1] $R^{\bullet}$ is a tryptophan radical (Sivaraja *et al.*, 1989; Huyett *et al.*, 1995). Compound I then is reduced back to the resting ferric (Fe^{3+}) state by the substrate, S, in two successive one-electron transfer events.

The crystal structures of several nonmammalian heme peroxidases now are known: cytochrome *c* peroxidase (CCP; Finzel *et al*., 1984), lignin peroxidase (Poulos *et al*., 1993), *Arthromyces ramosus* peroxidase (ARP; Kunishima *et al*., 1994), *Coprinus cinereus* peroxidase (Peterson *et al*., 1994), manganese peroxidase (Sundaramoorthy *et al*., 1994), peanut peroxidase (Schuller *et al*., 1996), and ascorbate peroxidase (APX; Patterson & Poulos, 1995). This structural information coupled with site-directed mutagenesis has provided considerable insight into the details of the peroxidase mechanism. The distal heme pocket forming the peroxide binding site contains a conserved histidine and an arginine residue which are required to promote the heterolytic fission of the peroxide O−O bond (Poulos & Fenna, 1994). The proximal pocket contains the invariant histidine heme ligand which forms a hydrogen bond with a conserved aspartate. Directly adjacent to the proximal His ligand is a nonpolar group which is Phe in most peroxidases. CCP has a tryptophan at this location, which is essential for enzyme activity (Mauro *et al*., 1988). Trp191 in CCP also is $R^{\bullet}$, the cation radical in compound I (Sivaraja *et al.*, 1989). The most straightforward explanation for why CCP forms a Trp

† This research was supported in part by the National Institutes of Health and the National Science Foundation.

* To whom correspondence should be addressed at the Department of Physiology & Biophysics. E-mail: poulos@uci.edu. Fax: (714) 824-8540.

‡ Present address: Room 236, Department of Structural Biology, Imperial Cancer Research Fund, 44 Lincoln's Inn Fields, London WC2A 3PX, U.K.

§ Present address: 201 Molecular Biology Institute, University of California at Los Angeles, Box 951570, Los Angeles, CA 90095-1570.

⊗ Abstract published in *Advance ACS Abstracts,* May 1, 1996.

[1] Abbreviations: CCP, cytochrome *c* peroxidase; APX, ascorbate peroxidase; EPR, electron paramagnetic resonance.

S0006-2960(96)00122-5 CCC: $12.00

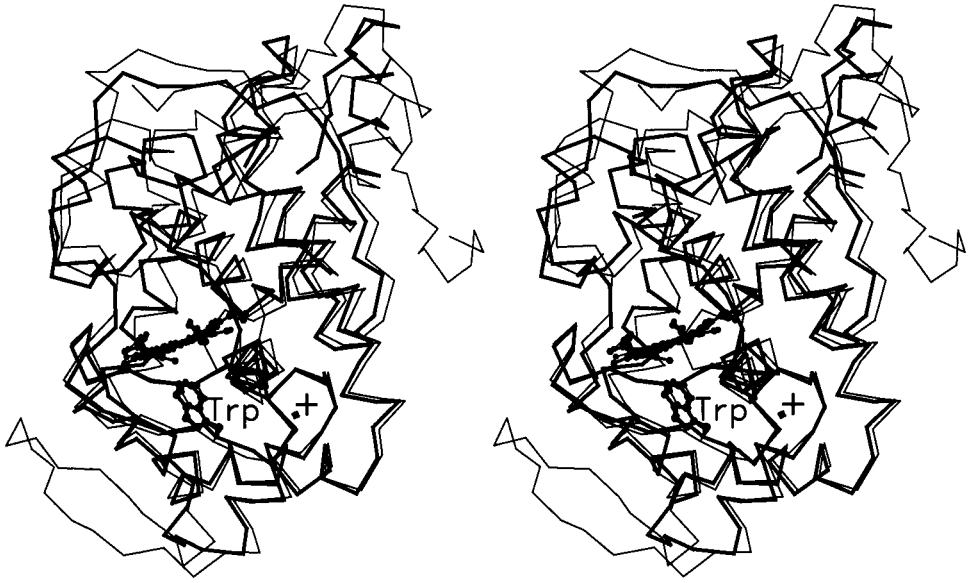

FIGURE 1: Stereodiagram of CCP (thin lines) superimposed on APX (thick lines). The proximal Trp residue (191 in CCP and 179 in APX), heme, and the APX cation are shown.

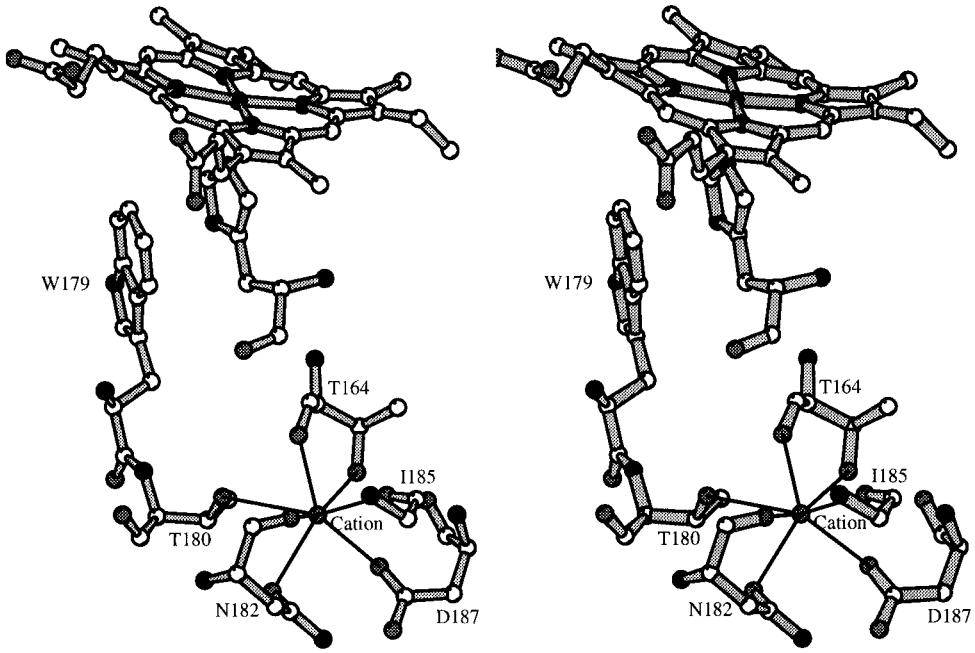

FIGURE 2: Stereomodel of the APX cation site. Oxygen atoms and the cation are gray, and nitrogen atoms are black. The thin lines highlight ligand−cation interactions.

rather than a porphyrin radical is that the proximal Trp is more easily oxidized than the proximal Phe found at this position in most other peroxidases.

As shown in Figure 1, the crystal structure of ascorbate peroxidase or APX (Patterson & Poulos, 1995) is very similar to that of CCP. In addition to containing the same catalytic residues, APX has a Trp (Trp179) in exactly the same location as Trp191 in CCP (Figure 1). Also like CCP, this proximal Trp in APX forms a hydrogen bond with a buried Asp. Therefore, it was anticipated that APX would form a CCP-like Trp radical in compound I. However, Patterson *et al*. (1995) showed that APX forms a porphyrin π cation radical and not a Trp radical as expected, while Pappa *et al*. (1996) found, by replacing the Trp with Phe, that the proximal Trp in APX is not essential for enzyme activity, as it is in CCP (Mauro *et al.*, 1988). Clearly, the explanation for what controls where the oxidizing equivalents in compound I reside is more complex than a single amino acid difference.

One obvious structural feature that separates CCP from APX is the presence of a cation binding site about 8 Å from the proximal Trp in APX. This cation binding site also is present in all five nonmammalian peroxidase structures, but absent in CCP (Figures 1 and 2). This site is occupied by calcium in most peroxidases but is thought to be occupied by potassium in APX (Patterson & Poulos, 1995). CCP and APX exhibit the same polypeptide conformation around the cation site (Figure 1), yet CCP lacks the appropriate side chains that can serve as cation ligands, so wild type CCP has a water molecule at this location rather than a cation. Patterson and Poulos (1995) have suggested that the presence of this cation in APX helps to increase the electrostatic potential in the proximal pocket which will destabilize a cation Trp radical in APX relative to CCP.

Because the polypeptide conformations of CCP and APX are the same in the vicinity of the proximal cation site (Figure 1), it appeared possible to introduce the APX proximal cation site into CCP by suitable multiple amino acid substitutions using site-directed mutagenesis. Therefore, we have constructed CCP mutants that contain the APX proximal cation site, and the mutants have been characterized using X-ray crystallography, stopped flow and steady state kinetics, and electron paramagnetic resonance spectroscopy. In brief, we find that the CCP mutants have a cation bound at the engineered site, exhibit greatly diminished ferrocytochrome *c* peroxidase activity, and do not generate a stable Trp191 radical. These results illustrate the importance of long range electrostatic effects in controlling where the oxidizing equivalents will reside in peroxidases and, most likely, in other redox enzymes.

MATERIALS AND METHODS

Materials. Enzymes for mutagenesis experiments were purchased from Boeringer Mannheim and New England Biolabs. Chromatography columns and media were purchased from Pharmacia Biotech. Horse heart cytochrome *c* was purchased from Sigma Chemical Co. and yeast cytochrome *c* was kindly provided by Dr. T. Yonetani. Hydrogen peroxide as a 30% w/v stabilized solution was obtained from Sigma. All other chemicals were purchased from Fisher Scientific and Sigma.

Mutagenesis. Oligonucleotide site-directed mutagenesis using the method of Kunkel *et al.* (1987) was performed on a modified pT7-7 vector that contained the cloned wild type CCP gene (Darwish *et al.*, 1991) as previously described by Choudhury *et al.* (1994). The CCP stop codon, TAG, was changed to TAA for a concurrent project. Two separate oligonucleotides (Operon Technologies) were annealed to the single-stranded uracyl-encoded CCP template. The 23mer, 5′-GGG GCT CAC ACC CTG GGC AAG AC-3′, changed Ala176 to Thr. The 48mer, 5′-GGT CCA TGG ACG GCC AAT AAC AAC GTC TTT GAC AAT TCG TTT TAC TTG-3′, changed Gly192, Ala194, Thr199, and Glu201 to the corresponding residues in APX: Thr, Asn, Asp, and Ser, respectively. All constructs were sequenced to verify DNA changes using Promega's thermal cycle sequencing. For unknown reasons, the first construct did not have the Glu201Ser mutation but the protein, mutant I, was expressed and analyzed. Subsequently, PCR using the 48mer and a downstream primer on the mutant I DNA template repaired the 201 position, generating mutant II which contained Ser at that position.

Protein Expression and Purification. The mutant recombinant CCPs were expressed in *Escherichia coli* BL21 cells and purified as previously described by Fishel *et al.* (1987) and Choudhury *et al.* (1994) using the same conditions as for the wild type enzyme. These proteins were twice crystallized by dialysis against Milli-Q water before being stored at −80 °C. The CCP concentration was estimated spectrophotometrically using an extinction coefficient at 408 nm of 96 mM^{-1} cm^{-1}.

Steady State Activity Assay. The steady state oxidation of horse heart cytochrome *c* was measured at 22 °C in a Cary 3E spectrophotometer by following the oxidation of ferrocytochrome *c* using an ΔA_{550nm} of 19 600 M^{-1} cm^{-1}. Typical final reaction conditions consisted of 40 μM dithionite-reduced horse heart ferrocytochrome *c*, 180 μM H_2O_2, 75 nM mutant I or II, or 50 pM wild type CCP, in 50 mM potassium phosphate and 1 mM EDTA (pH 6.0) (Yonetani, 1966). Hydrogen peroxide stocks were standardized with $KMnO_4$ using the method of Fowler and Bright (1935).

The ability of mutants I and II to oxidize small molecule substrates was determined using guaiacol and potassium ferrocyanide as substrates. The guaiacol peroxidase activity was determined in 50 mM potassium phosphate pH 7.0 containing 100 mM guaiacol, 600 μM H_2O_2, and 75 nM mutant or wild type CCP (Miller *et al.*, 1992). The formation of the oxidized product, tetraguaiacol, was followed at 470 nm using an extinction coefficient of 26 600 M^{-1} cm^{-1}. Ferrocyanide peroxidase activity was determined in 1 mL spectrophotometer cells containing 17 mM $K_4Fe(CN)_6 \cdot 3H_2O$, 600 μM H_2O_2, and 75 nM mutant or wild type CCP in 100 mM potassium phosphate (pH 6.0) (Mauro *et al.*, 1988). The formation of the oxidized product, ferricyanide, was monitored at 420 nm using an extinction coefficient = 1000 M^{-1} cm^{-1}.

Stopped Flow Kinetics. In order to evaluate if the mutant CCPs would form a porphyrin cation radical when reacted with H_2O_2 to form compound I, stopped flow kinetics were measured using a High Tech model SF-51 stopped flow instrument linked to a Hi-Tech SU-40 spectrophotometer with a 1 cm path length cell. The output was monitored and recorded on a Compaq personal computer for kinetic analysis. Compound I formation was followed at 425 nm by mixing 1.4 μM CCP with 8.4 μM H_2O_2 in 20 mM potassium phosphate (pH 6.0). Kinetic analysis was performed using the Hitech IS-1 software suite version 1.0.

Electron Paramagnetic Resonance. EPR spectra for wild type and mutant CCPs were recorded on a Bruker ESP300 spectrometer equipped with an air products LTR3 liquid helium cryostat. The following instrument settings were used: microwave frequency, 9.52 GHz; microwave power, 50.0 mW; modulation amplitude, 4.63 G; modulation frequency, 100 kHz; field sweep rate, 47.6 G/s; time constant, 0.082 s; and gain, 2.0×10^3. The resting state sample had mutant or wild type CCP at 300 μM in 50 mM potassium phosphate (pH 6.0) in a total volume of 0.3 mL. Compound I was formed by the addition of H_2O_2 to 360 μM. Samples were quickly frozen in quartz EPR tubes by submersion in liquid nitrogen over a period of 90 s, and spectra were recorded at 7.5 K.

Crystallization, X-ray Data Collection, and Structure Refinement. Diffraction quality crystals were prepared in 30% 2-methyl-2,4-pentanediol and 50 mM potassium phosphate (pH 6.0) according to Edwards and Poulos (1990), with modifications described by Sundaramoorthy *et al.* (1991). The concentration used for mutant I was 16 mg/mL, while mutant II required a higher protein concentration (21 mg/mL) and greater care to crystallize since this mutant tended to be less stable. X-ray intensity data were collected using a Siemens area detector system and a rotating anode X-ray source equipped with focusing optics. A single crystal was used for each data set and a summary of data collection is provided in Table 1. The mutant crystals tended to be less stable in the X-ray beam with greater mosaic spread which accounts for the relatively large scaling R_{merge} compared to what typically is obtained for native CCP crystals. The structures were refined with conventional positional refine-

Table 1: Summary of X-ray Intensity Data Collection and Crystallographic Refinement

	mutant 1	mutant 2
total no. of observations	171 560	122 386
no. of independent reflections	17 919	21 248
$I/\sigma I$ at the highest resolution	1.05 at 2.4 Å	1.0 at 2.2 Å
R_{merge} (%)[a]	13.07	14.04
completeness of all data (%)	99	90
highest-resolution shell (%)	99 between 2.55 and 2.40 Å	84 between 2.3 and 2.2 Å
no. of reflns used in refinement $F > 2\sigma(F)$ to 2.4 Å	14 765	14 727
$R = \Sigma\|\|F_o\|-\|F_c\|\|/\Sigma\|F_o\|$ (%)	19.3	23.4
rms in bond lengths (Å)	0.008	0.009
rm in bond angles (deg)	1.64	1.72

[a] $R_{merge} = \Sigma|I_i-\langle I_i\rangle|/\Sigma I_i$ where I_i = intensity of the ith observation and $\langle I_i\rangle$ mean intensity.

ment using X-PLOR (Brunger, 1992). The initial difference maps were computed using phases obtained from the wild type model but with the mutated side chains removed. The new side chains were fit to the $F_o - F_c$ and $2F_o - F_c$ electron density maps, followed by refinement. At this stage, the cation site was introduced into the model. A summary of crystallographic refinement statistics is shown in Table 1.

Electrostatic Calculations. Electrostatic potential calculations were carried out with the DELPHI program as implemented in the Biosym INSIGHT package. One of the requirements of the calculation is to center the protein in a large box that encompasses both the protein and surrounding solvent to be included in the calculation. The box is divided into a three-dimensional grid (1 Å per grid point) and the electrostatic potential evaluated at each grid point. It was important for direct comparisons that the same grid be used for all protein models. Therefore, the same grid used for wild type CCP was used for the mutants and APX. The mutant protein crystals had the CCP molecule in the asymmetric unit slightly translated relative to the wild type crystals so it was necessary to first superimpose the mutant structures onto the wild type structure. For placement of APX into the same grid box, the heme of APX was superimposed onto the CCP heme and the resulting rotation/translation matrix applied to the rest of the protein. Partial charges were assigned to protein atoms using the united atom approximation in the AMBER (Weiner *et al.*, 1984) charge set provided by Biosym. The heme and His ligand charges were assigned according to Collins and Loew (1992). Care was taken with histidine residues to ensure that the ring nitrogen carrying the proton was consistent with the local electrostatic environment. For CCP, this meant placing the proton on NE2 of His96 and ND1 of His6, -52, and -96. Two protons were placed on His181, giving a net positive charge (Miller *et al*., 1994a,b) since His181 sits between and makes contact with a heme propionate and an Asp residue. For APX, the proton was placed on ND1 for His42, -163, and -169 and NE1 for His62, -68, -116, -140 and -239. The external dielectric was set to 80 with an ionic strength of 0.1, while the internal dielectric of the protein was set to 9.0 (Aqvist *et al*., 1991). The internal dielectric is the major unknown in these calculations. However, the choice of what to use for the internal dielectric changes only the absolute magnitude of the differences between protein models and not the relative differences.

RESULTS

Initial Characterization. The CCP mutants exhibited spectral properties characteristic of the wild type enzyme (Figure 3). Addition of 1 equiv H_2O_2 gave the expected shift in the visible absorption spectrum from 408 to 419 nm characteristic of the Fe^{4+}═O center (Figure 3). The stability of the Fe^{4+}═O center can be estimated by following the change in the spectrum as a function of time as Fe^{4+}═O is reduced to the Fe^{3+} state. The mutant II compound I spectrum shifts back toward the resting state spectrum in about 15−20 min, while the wild type enzyme takes on the order of hours. Hence, it appears that the Fe^{4+}═O center is less stable in the mutant.

Crystal Structures. The crystal structures of mutants I and II initially were refined without the mutant side chains or cation included. After a few rounds of positional refinement, the side chains were introduced into the model and the model again was refined using conventional positional refinement. At this stage, an $F_o - F_c$ electron density map in the vicinity of the cation binding loop was examined and water placed in a difference peak approximately 10 times above background at the cation site. During further refinement of mutant I, the B factor for the water dropped to 2 Å^2, the minimum allowed by the program, and a large positive difference peak still appeared at the cation site. Introduction of a cation modeled as potassium at this site followed by positional and temperature factor refinement yielded a flat $F_o - F_c$ difference map with a cation B factor of 14 Å^2. The cation site behaved similarly during refinement of mutant II. Shown in Figure 4 are omit $F_o - F_c$ electron density difference maps where the side chains of the ligands and cation were removed from the model followed by several rounds of refinement. These data clearly show that this site now is occupied by a cation exactly as it is in all other known plant and fungal peroxidase structures. The changes in both mutant structures are confined to the cation site, with no observable changes in the active site, including the position and local environment around Trp191.

Mutant I had residues 176, 192, 194, and 199 converted to the corresponding residues in APX: Thr, Thr, Asp, and Asn, respectively. Mutant II had these changes plus Glu201 converted to Ser, the corresponding residue in APX. For reasons which remain unknown, mutant I retained a Glu at position 201. In modeling the cation site for mutant I before protein expression, we noted that Glu201 might sterically hinder the ability of Asn194 to coordinate with the cation. This prediction was confirmed by the X-ray structure of mutant I. Asn194 does not coordinate with the cation in mutant I because Glu201 forces Asn194 to point out and away from the cation (Figure 4). Subsequently, Glu201 was converted to the corresponding residue in APX, Ser, in order to eliminate this steric interference and allow the Asn194−cation ligation interaction. As expected, the Asn194 side chain in mutant II rotated in to coordinate with the cation (Figure 4). Although the preparation of mutant II was our primary goal, it was fortunate that we chose to proceed with an analysis of mutant I. This mutant shares all the functional and spectroscopic properties with mutant II but is a more stable protein and more readily crystallized. The omit electron density map in Figure 4 shows that the only differences between the two mutants are the Asn194 side chain position and the fact that Glu201 is replaced by Ser.

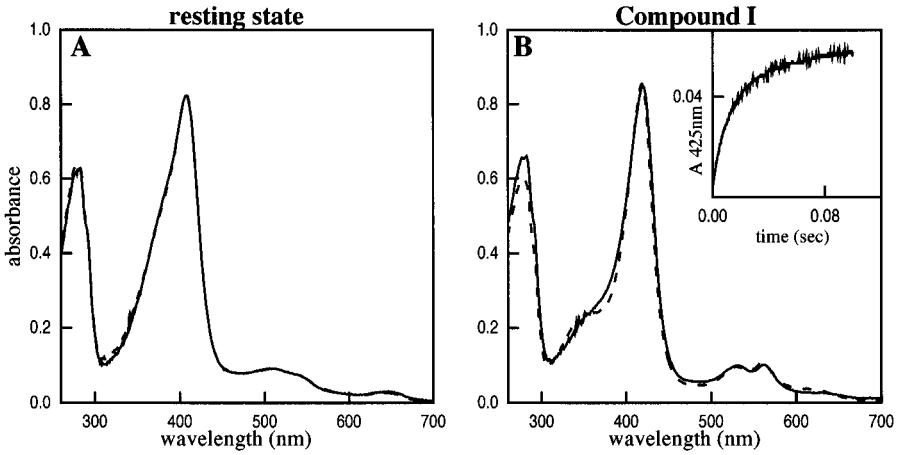

FIGURE 3: Absorption spectra of wild type CCP (dotted lines) and mutant II (solid lines): (A) resting state and (B) compound I. The inset in B is the stopped flow trace when 1.4 μM mutant II is mixed with 8.4 μM H_2O_2. The absence of a decrease in absorbance indicates that a porphyrin π cation radical does not form on the time scale of the stopped flow experiment.

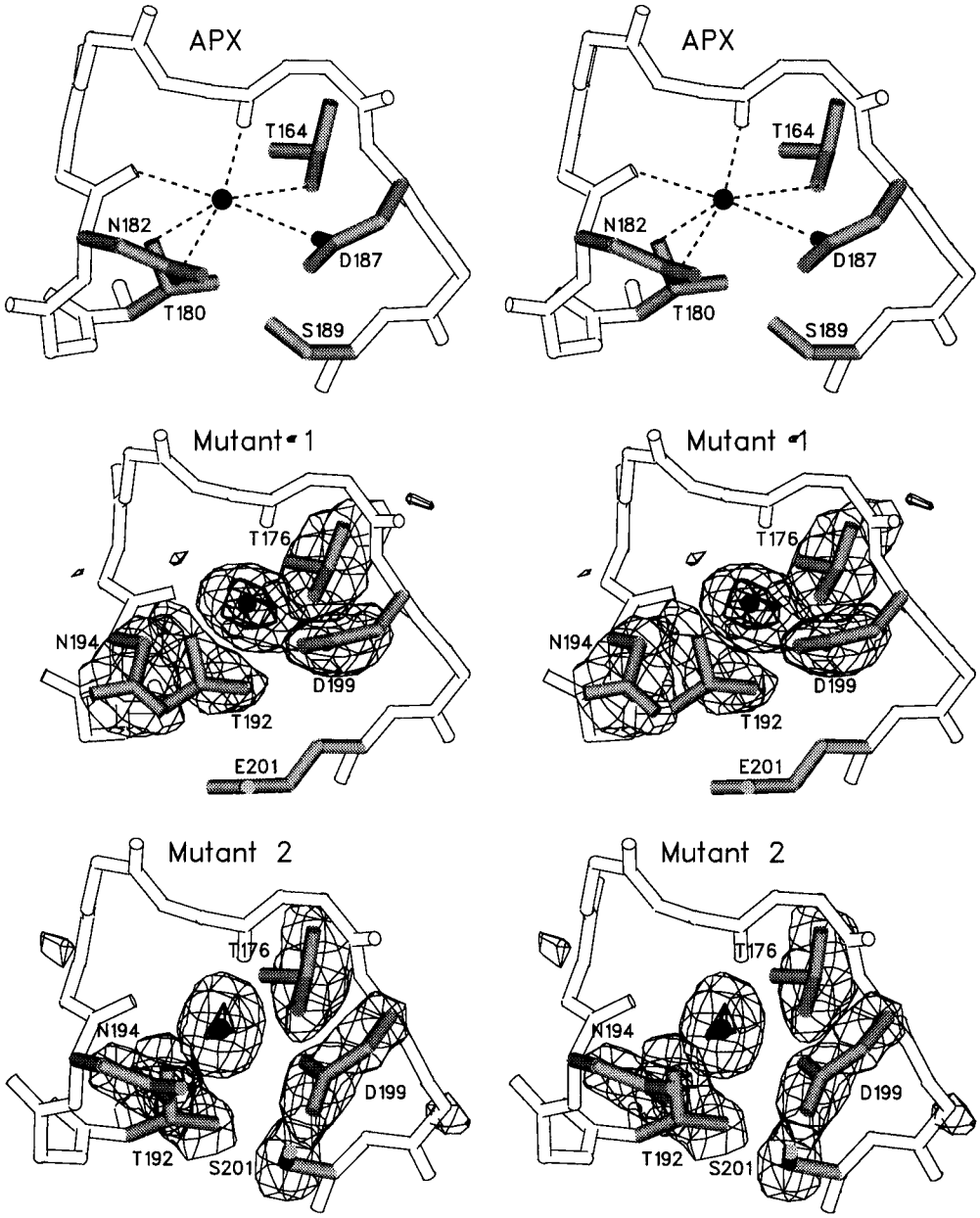

FIGURE 4: Stereoscopic diagrams of the $F_o - F_c$ electron density maps. For comparison, the APX cation site and its interaction with protein ligands also are shown. The maps were contoured at $+3\sigma$ (thin lines) and $+10\sigma$ (thick lines). The ligand side chains and cation were removed from the models prior to several rounds of refinement and electron density map calculations. The side chains are highlighted in gray.

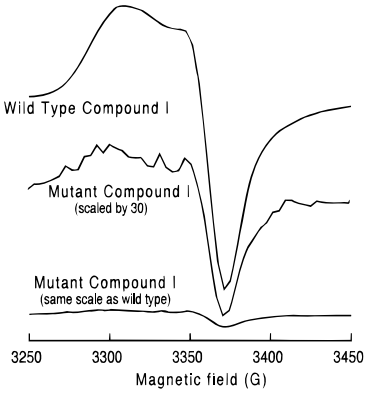

FIGURE 5: Derivative EPR spectrum (7.5 K) of wild type CCP and mutant I. Mutant II behaves the same as mutant I. The experimental conditions are given in Materials and Methods.

Hence, the coordination environment in mutant II is now exactly the same as in APX (Figures 2 and 4).

EPR Spectroscopy. The EPR spectra of compound I for wild type and mutant I are shown in Figure 5. The samples were prepared by the addition of a slight excess of H_2O_2 over enzyme followed by immediate freezing in liquid nitrogen. The characteristic wild type Trp191 radical EPR signal is shown in Figure 5 and on the same scale, the mutant shows only a trace of a signal. If the scale is expanded 30-fold, the signal for the mutants is very similar to that expected for the Trp191 radical but clearly is only a fraction of the signal observed in the wild type enzyme. This indicates that mutant I initially forms a Trp191 radical, but the radical is much less stable than in wild type CCP. Mutant II behaved exactly the same as mutant I.

Electrostatic Calculations. Replacement of Trp191 with Gly in CCP leaves a large hole that the crystal structure shows is partially occupied with a cation (Miller *et al*., 1994a,b). This, together with electrostatic calculations, indicates that the proximal pocket in CCP is uniquely suited to stabilize the Trp191 cation radical (Miller *et al*., 1994a,b). If the engineered cation in CCP destabilizes a Trp cation radical by increasing the electrostatic potential in the vicinity of Trp191, this should be reflected in the calculated electrostatic potential. A comparison of the electrostatic potentials in the vicinity of Trp191 among CCP, APX, and the CCP mutants is shown in Table 2. The electrostatic potential in the cation-containing CCP mutants is more positive than in wild type CCP. To assess the effect of the potassium ion in APX, the calculation was repeated for the APX model except the potassium ion was excluded from the model. A comparison of the various averaged values in Table 2 indicates that the cation accounts for about half of the more positive electrostatic environment around the proximal Trp in APX compared to CCP.

Enzyme Activity. On the basis of the EPR results, we anticipated that the radical in the mutant CCP might now reside on the porphyrin. This should be relatively easy to see in the stopped flow since oxidation of the porphyrin leads to a large decrease in the Soret maximum of the visible absorption spectrum. The Trp191-to-Phe (Erman *et al*., 1989) and the proximal His175 ligand-to-Gln and Trp191-to-Phe double mutant (Choudhury *et al*., 1994) both lead to the formation of compound I porphyrin radicals readily detectable using stopped flow methods. Therefore, one should be able to observe a rapid decrease in absorbance when peroxide is mixed with the mutant rather than the normal increase in absorbance if a porphyrin radical is formed. However, what we observe is an increase (Figure 3, inset) very similar to what is observed in wild type CCP. The second-order rate of compound I formation = $(1.8 \pm 0.07) \times 10^7$ M^{-1} s^{-1} compared with various published values for recombinant CCP, 3.03×10^7 M^{-1} s^{-1} (Goodin et al., 1991) and 4.5×10^7 M^{-1} s^{-1} (Erman et al., 1993). Therefore, the mutant CCP appears not to form a porphyrin cation radical on the time scale of the stopped flow experiment.

Table 2: Calculated Electrostatic Potential at the Position of the Indicated Indole Ring Atom

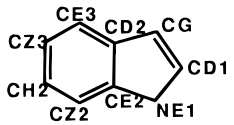

	electrostatic potential (kcal/mol)				
indole atom	CCP	APX	APX (no K^+)	mutant I	mutant II
CG	−8.79	−4.26	−5.69	−5.18	−5.13
CD1	−8.53	−2.97	−4.09	−4.78	−5.26
CD2	−20.52	−11.76	−13.02	−18.48	−18.73
NE1	−14.29	−14.82	−15.73	−13.60	−15.80
CE2	−13.67	−10.15	−11.11	−12.80	−11.00
CE3	−5.01	−3.50	−4.84	−5.85	−5.00
CZ2	−6.01	−3.39	−4.17	−5.66	−4.83
CZ3	−11.07	−3.53	−4.57	−5.38	−6.14
CH2	−4.97	−1.70	−2.51	−4.32	−2.46
average	−10.32	−6.23	−7.30	−8.45	−8.26

Table 3: Steady State Activities of Wild Type and Mutant Enzymes Using Different Substrates[a]

enzyme	substrate	k_{cat} (s^{-1})
wild type	ferrocytochrome c	581 ± 95 (8)
mutant I	ferrocytochrome c	1.0 ± 0.10 (7)
mutant II	ferrocytochrome c	0.73 ± 0.10 (8)
wild type	guaiacol	5.23 ± 1.38 (5)
mutant I	guaiacol	13.28 ± 0.98 (5)
mutant II	guaiacol	13.06 ± 1.16 (5)
wild type	ferrocyanide	145.52 ± 17.9 (5)
mutant I	ferrocyanide	8.24 ± 0.63 (5)
mutant II	ferrocyanide	7.12 ± 0.63 (5)

[a] The experimental conditions are given in Materials and Methods. The numbers in parentheses are the number of assays used for determination of standard deviations.

The steady state activity was determined using horse heart ferrocytochrome *c* and two small molecule substrates, guaiacol and potassium ferrocyanide (Table 3). The mutants exhibit <1% of wild type levels of ferrocytochrome *c* peroxidase activity, while the activity toward guaiacol has increased. These results, coupled with the stopped flow work, show that the peroxide fission mechanism is still intact but that the ability to oxidize ferrocytochrome *c* is greatly diminished.

DISCUSSION

Crystal Structures. The crystal structures show that engineering the APX cation ligands into CCP results in the binding of a cation to CCP mutants I and II. The polypeptide

conformations forming the cation site in CCP, APX, and other fungal and plant peroxidases are very similar, thus permitting multiple amino acid substitutions without significant changes in polypeptide conformation. Most importantly, the active site structures including the immediate environment around Trp191 are not perturbed.

Stability of the Trp191 Radical. The hypothesis being tested in this work is whether the proximal cation in peroxidases can influence the stability and location of the organic radical formed in compound I. The electrostatic calculations indicate that the mutant cation site does increase the electrostatic potential in the immediate vicinity of Trp191 even though the cation is ≈8 Å from the nearest Trp atom. Most importantly, the EPR data show that the mutants form a much less stable Trp191 radical. The shape of the EPR signal, although much weaker than that of wild type CCP, still indicates a small fraction of spin density on Trp191. This observation, coupled with the stopped flow work, indicates that the mutants do not form an APX-like porphyrin π cation radical in compound I. The initial reaction between peroxide and the mutants probably results in the formation of a transient Trp191 radical which rapidly disproportionates, resulting in the oxidation of other sites (Fishel et al., 1991), perhaps neighboring tyrosines. The main effect of the cation is to greatly lower the stability of the Trp191 radical, but the cation appears not to prevent Trp191 from serving as the initial site of oxidation. As the electrostatic calculations indicate (Table 2), the new cation accounts for about half of the more positive electrostatic potential around the proximal Trp in APX compared to CCP. Because the polypeptide conformations are so similar in CCP and APX, the remaining two-thirds of the difference in the Trp191 electrostatic environment must be controlled by side chain differences. Preliminary calculations on modeled CCP mutants indicate that no simple single mutation will alter the electrostatic environment of CCP to more closely resemble that of APX. CCP contains Met and Tyr residues in the vicinity of Trp191, while APX does not. The heme propionates in APX are anchored in place by an Arg residue, while the corresponding residue in CCP is Asn. Hence, CCP contains more electronegative atoms and fewer positively charged side chains surrounding the proximal pocket. Stabilization of the Trp191 cation radical very likely involves many long range and complex electrostatic effects. Despite this probable complexity, it is clear that a single new cation site greatly decreases the stability of the Trp191 radical.

Enzyme Activity. The activity of the CCP mutants harboring the new cation closely parallels the activity profiles of the Trp191Phe mutant (Mauro *et al.*, 1988). In the cation mutants, the ferrocytochrome *c* and ferrocyanide peroxidase activities are, respectively, ≈0.02 and ≈5% of wild type levels. The corresponding values for the Phe191 mutant were reported to be 0.028 and 12.5% (Mauro *et al.*, 1988). However, the guaiacol peroxidase activity in the cation mutants is about 2.5-fold higher compared to that of the wild type. These observations are consistent with current views on how small and large molecules are oxidized by peroxidases. Small molecule substrates, like guaiacol, are thought to deliver an electron to the exposed heme edge (Depillis et al., 1991). This region is not altered in the cation mutants. In contrast, cytochrome *c* is restricted to interact with the CCP surface and not the CCP heme edge. The crystal structures of CCP complexed with horse and yeast cytochrome *c* have been solved (Pelleiter & Kraut, 1992), and there now is growing evidence that the Pelletier−Kraut model represents the primary site of interaction (Miller *et al.*, 1994a,b; Pappa & Poulos, 1995). Trp191 is situated along the direct route between the two heme centers in the Pelletier−Kraut model, indicating that Trp191 might be the primary electron-accepting site for ferrocytochrome *c* oxidation.

Ferrocyanide may act through the same path as cytochrome *c*. Ferrocyanide, unlike guaiacol, is a polar charged molecule that may not be able to access the same site as guaiacol, the exposed heme edge. If ferrocyanide interacts with the CCP surface and utilizes the same electron transfer path as ferrocytochrome *c*, the low ferrocyanide peroxidase activity would be explained. The increase in activity toward guaiacol could be due to an increase in reactivity of the Fe^{4+}=O center, as shown by the relative instability of the Fe^{4+}=O spectrum compared to that of wild type compound I, and the ability of guaiacol to approach close to the heme edge. Additionally, there is an oxidizing equivalent present in compound I of the mutants that is on neither Trp191 nor the porphyrin. Since the Trp191 radical is so unstable in the mutants, the Trp191 oxidizing equivalent rapidly migrates elsewhere in the protein (tyrosines?), which could provide additional centers for guaiacol oxidation on the enzyme surface.

The above discussion leads to the conclusion that the introduction of the cation results in a specific loss in ferrocytochrome *c* peroxidase activity because Trp191 no longer can form a stable cation radical as it does in wild type CCP. The cation increases the electrostatic potential surrounding Trp191, and the proximal environment no longer is able to effectively stabilize a cationic Trp radical. This correlates well with the recent findings that changing Trp191 to Gly enables a cation, including imidazolium cations, to enter into the space vacated by Trp191 because this region of CCP is designed to stabilize a positive charge (Miller *et al.*, 1994a,b; Fitzgerald *et al.*, 1994, 1995). The different environment around CCP's Trp191 alters the electrostatic potential from that of Trp179 in APX. Another possibility is that the cation interferes with the interaction between CCP and cytochrome *c*. In Figure 6 is shown the Pelletier−Kraut model of the intramolecular complex and the location of the engineered cation. The cation is not close to any of the intramolecular electrostatic contacts between the two proteins so it is unlikely that the cation directly interferes with complex formation. However, the cation is close to the section of polypeptide that is the proposed direct route of electron transfer from the cytochrome *c* heme to Trp191 in CCP (Figure 6; Pelletier & Kraut, 1992). For example, the backbone of Ala194 in CCP is 4 Å from the cytochrome *c* heme, and Ala194 was converted to Thr to form a cation ligand. Hence, it could be possible that the cation alters the electrostatic properties on the proposed electron transfer pathway as well as destabilizes the Trp191 cation radical.

These observations suggest that Trp191 serves as more than a conduit between ferrocytochrome *c* and CCP heme iron atoms but that the oxidation/reduction of Trp191 is an essential part of the electron transfer reaction. Scheme 1 outlines the simplest mechanism consistent with this idea (Hahm *et al.*, 1994; Liu *et al.*, 1994).

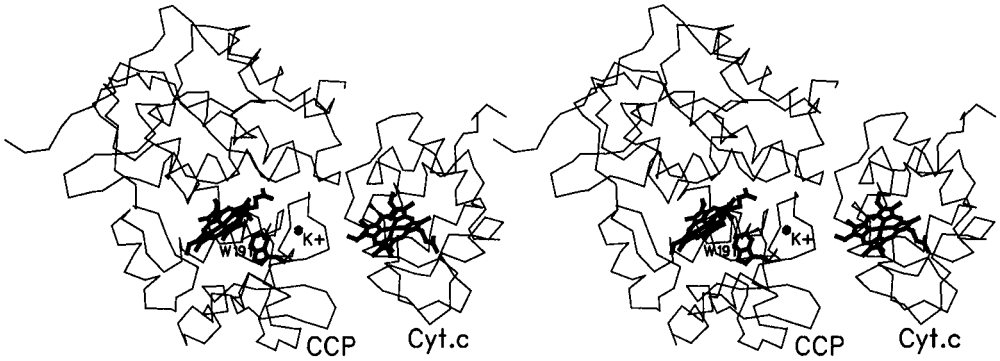

FIGURE 6: Stereo diagram of the Pelletier−Kraut CCP−cytochrome *c* noncovalent complex (2pcc.pdb) showing the location of the engineered cation site (labeled K+).

Scheme 1

$$\underset{\text{compound I}}{Fe^{4+}{=}OTrp^{\bullet}} \rightarrow \underset{\text{compound II}}{Fe^{4+}{=}OTrp} \rightarrow Fe^{3+}Trp^{\bullet} \rightarrow Fe^{3+}Trp$$

Scheme 1 requires that Trp191 be able to reduce the Fe^{4+}═O center in an intramolecular electron transfer reaction. Consistent with this scheme is a pH-dependent rapid equilibration between the radical and Fe^{4+}═O (Coulson *et al*., 1971) which is supported by more recent work (Hahm *et al*., 1994). The primary drawback of this mechanism is that the estimated intramolecular electron transfer rate from Trp191 to Fe^{4+}═O is too slow to account for the steady state rate (Ho *et al*., 1983), although a mechanism has been proposed where conformational gating in the CCP−cytochrome *c* complex enables the Trp-to-Fe^{4+}═O electron transfer reaction to proceed rapidly (Ho *et al*., 1983). However, in some cases, it is Fe^{4+}═O and not the Trp191 radical that is reduced. Both stopped flow (Nuevo *et al*., 1993; Hahm *et al*., 1993; Matthis & Erman, 1995) and rapid photoreduction techniques (Hazzard & Tollin, 1991) show that the Fe^{4+}═O is preferentially reduced first at low ionic strengths and the Trp191 radical at high ionic strengths. This raises the possibility that different sites of interaction between CCP and ferrocytochrome *c* lead to the reduction of the Trp191 radical or Fe^{4+}═O centers. Even if we postulate two sites, it is difficult to eliminate the involvement of Trp191 in the reduction of the Fe^{4+}═O center since the Trp191-to-Phe mutant is inactive (Mauro *et al*., 1988) as are the cation mutants described in the present study. If an electron can be delivered to the Fe^{4+}═O center without the involvement of Trp191, we would expect these mutants to exhibit reasonable levels of activity, but obviously this is not the case. Overall, the one picture most consistent with the available and most recent data (Liu *et al*., 1994) points to Scheme 1 as the primary reaction mechanism.

Summary. It is clear that there are some important remaining puzzles and inconsistencies in the CCP−cytochrome *c* system. Nevertheless, the present work allows us to draw two main conclusions. First, the ability to oxidize Trp191 and form a stable Trp191 cation radical is important for activity. Second, the cation mutants have shown that long range electrostatic interactions can have a profound effect on a redox active amino acid which very likely will be of relevance in other metalloproteins.

ACKNOWLEDGMENT

We thank Dr. Li Ma for assistance with the EPR experiments.

REFERENCES

Aqvist, J., Luecke, H., Quiocho, F. A., & Warshel, A. (1991) *Proc. Natl. Acad. Sci. U.S.A. 88*, 2026−2030.
Brunger, A. (1992) *X-PLOR 3.1*, Yale University Press, New Haven, CT.
Choudhury, K., Sundaramoorthy, M., Hickman, A., Yonetani, T., Woehl, E., Dunn, M.F., & Poulos, T. L. (1994) *J. Biol. Chem. 269*, 20239−20249.
Collins, J. R., & Loew, G. H. J. (1992) *Quantum Chem. Symp 19*, 87−107.
Coulson, A. F. W., Erman, J. E., & Yonetani, T. (1971) *J. Biol. Chem. 246*, 917−924.
Darwish, K., Li, H., & Poulos, T. L. (1991) *Protein Eng. 4*, 701−708.
DePillis, G. D., Sishta, B. P., Mauk, A. G., & Ortiz de Montellano, P. R. (1991) *J. Biol. Chem. 266*, 19334−19341.
Dolphin, D., Forman, A., Borg, D. C., Fajer, J., & Felton, R. H. (1971) *Proc. Natl. Acad. Sci. U.S.A. 68*, 614−618.
Edwards, S. E., & Poulos, T. L. (1991) *J. Biol. Chem. 265*, 2588−2595.
Erman, J. E., Kim, K. L., Vitello, L. B., Moench, S. J., & Saterlee, J. D. (1987) *Biochim. Biophys. Acta 911*, 1−10.
Erman, J. E, Vitello, L. B., Miller, M. A., & Kraut, J. (1992) *J. Am. Chem. Soc. 114*, 6592−6593.
Erman, J. E., Vitello, L. B., Miller, M. A., Shaw, A., Brown, K. A., & Kraut,J. (1993) *Biochemistry 32*, 9798−9806.
Finzel, B. C., Poulos, T. L., & Kraut, J. (1984) *J. Biol. Chem. 259*, 13027−13036.
Fishel, L. A., Villafranca, J. E., Mauro, M. J., & Kraut, J. (1987) *Biochemistry 26*, 351−360.
Fishel, L. A., Farnum, M. F., Mauro, J. M., Miller, M. A., & Kraut, J. (1991) *Biochemistry 30*, 1986−1996.
Fitzgerald, M. M., Churchill, M. J., McRee, D. E., & Goodin, D. B. (1994) *Biochemistry 33*, 3807−3818.
Fitzgerald, M., Trester, M. L., Jensen, G. M., McRee, D., & Goodin, D. B. (1995) *Protein Sci. 4*, 1844−1850.
Fowler, R. M., & Bright, H. A. (1935) *J. Res. Natl. Bur. Stand. 15*, 493−575.
Goodin, D. B., Davidson, M. G., Roe, J. A., Mauk, A. G., & Smith, M. (1991) *Biochemistry 30*, 4953−4962.
Hahm, S., Green, L., Durham, B., & Millet, F. (1993) *J. Am. Chem. Soc. 115*, 3372−3373.
Hahm, S., Miller, M. A., Geren, L., Kraut, J., Durham, B., & Millett, F. (1994) *Biochemistry 33*, 1473−1480.
Hazzard, J. T., & Tollin, G. (1991) *J. Am. Chem. Soc. 113*, 8956−8957.
Ho, P. S., Hoffman, B. M., Kang, C. H., Margoliash, E. (1983) *J. Biol. Chem. 258*, 4356−4363.
Huyett, J. E., Doan, P. E., Gurbriel, R., Houseman, A. L. P., Sivaraja, M., Goodin, D. B., & Hoffman, B. M. (1995) *J. Am. Chem. Soc. 117*, 9033−9041.
Kunishima, N., Fukuyama, K., Matsubara, H., Hatanaka, H., Shibano, Y., & Amachi, T. (1994) *J. Mol. Biol. 235*, 331−344.
Kunkel, T. A., Roberts, J. D., & Zokour, R. A. (1987) *Methods Enzymol. 154*, 367−382.
Liu, R.-Q., Miller, M. A., Han, G. W., Hahm, S., Green, L., Hibdon, S., Kraut, J., & Millett, F. (1994) *Biochemistry 33*, 8678−8685.

Matthis, A. L., & Erman, J. E. (1995) *Biochemistry 34*, 9985−9990.

Mauro, M. J., Fishel, L. A., Hazzard, J. T., Meyer, T. E., Tollin, G., Cusanovich, M.A., & Kraut, J. (1988) *Biochemistry 27*, 6243−6256.

Miller, M. A., Liu, R.-Q., Hahm, S., Geren, L., Hibdon, S., Kraut, J., Durham, B., & Millett, F. (1994a) *Biochemistry 33*, 8686−8693.

Miller, M. A., Han, G. W., & Kraut, J. (1994b) *Proc. Natl. Acad. Sci. U.S.A. 91*, 11118−11122.

Miller, V. P., Depillis, G. D., Ferrer, J. C., Mauk, A. G., & Ortiz de Montellano, P. R. (1992) *J. Biol. Chem 267*, 8936−8942.

Nuevo, M. R., Chu, H.-H., Vitello, L. B., & Erman, J. E. (1993) *J. Am. Chem. Soc. 115*, 5873−5874.

Pappa, H., & Poulos, T. L. (1995) *Biochemistry 34*, 6573−6580.

Pappa, H., Patterson,W. R., & Poulos,T. L. (1996) *J. Bioinorg. Chem. 1*, 61−66.

Patterson, W. R., & Poulos, T. L. (1995) *Biochemistry 34*, 4331−4341.

Pattereson, W. R., Poulos, T. L., & Goodin, D. B. (1995) *Biochemistry 34*, 4342−4345.

Pelletier, H., & Kraut, J. (1992) *Science 258*, 1748−1755.

Peterson, J. F. W., Kaziola, A., & Larsen, S. (1994) *FEBS Lett. 339*, 291−296.

Poulos, T. L., & Fenna, R. E. (1994) *Met. Biol. 30*, 25−75.

Poulos, T. L., Edwards, S. L., Wariishi, H., & Gold, M. H. (1993) *J. Biol. Chem. 268*, 4429−4440.

Schuller, D. J., Ban, N., van Huystee, R. B., McPherson A., & Poulos, T. L. (1996) *Structure* (in press).

Sivaraja, M., Goodin, D. B., Smith, M., & Hoffman, B. M. (1989) *Science 245*, 738−740.

Sundaramoorthy, M., Choudhury, K., Edwards, S. L., & Poulos, T. L. (1991) *J. Am. Chem. Soc. 113*, 7755−7757.

Sundaramoorthy, M., Katsuyuki, K., Gold, M. H., & Poulos, T. L. (1994) *J. Biol. Chem. 269*, 32759−32767.

Weiner, S. J., et al. (1984) *J. Am. Chem. Soc. 106*, 765−784.

Yonetani, T.(1966) *Biochem. Prep. 11*, 14−20.

BI960122X